J Mater Sci (2009) 44:136–148
DOI 10.1007/s10853-008-3117-9

Microstructural phase evaluation of high-nitrogen Fe–Cr–Mn alloy powders synthesized by the mechanical alloying process

R. Amini · M. J. Hadianfard · E. Salahinejad · M. Marasi · T. Sritharan

Received: 14 August 2008 / Accepted: 12 November 2008 / Published online: 27 November 2008
© Springer Science+Business Media, LLC 2008

Abstract In this study, the formation of Fe18Cr8Mn*x*N alloys by mechanical alloying (MA) of the elemental powder mixtures was investigated by running the milling process under nitrogen and argon gas atmospheres. The effect of the milling atmosphere on the microstructure and phase contents of the as-milled powders was evaluated by X-ray diffraction and transmission electron microscopy. The thermal behavior of the alloyed powders was also studied by differential scanning calorimetry. The results revealed that in the samples milled under nitrogen, three different phases, namely ferrite (α), austenite (γ), and a considerable amount of amorphous phase are present in the microstructure. In contrast, in the samples milled under argon, the structure contains the dominant crystalline ferrite phase. By progression of MA under the nitrogen atmosphere, the ferrite-to-austenite phase transformation occurs; meanwhile, the quantity and stability of the amorphous phase increase, becoming the dominant phase after 72 h and approaching 83.7 wt% within 144 h. The quantitative results also showed that by increasing the milling time, grain refinement occurs more significantly under the nitrogen atmosphere. It was realized that the infused nitrogen atoms enhance the grain refinement phenomenon and act as the main cause of the amorphization and α-to-γ phase transformation during MA. It was also found out that the dissolved nitrogen atoms suppress the crystallization of the amorphous phase during the heating cycle, thereby improving the thermal stability of the amorphous phase.

R. Amini (✉) · M. J. Hadianfard · E. Salahinejad · M. Marasi
Department of Materials Science and Engineering, School of Engineering, Shiraz University, Zand Blvd, 7134851154 Shiraz, Iran
e-mail: ramini2002@gmail.com

R. Amini · T. Sritharan
School of Materials Science and Engineering, Nanyang Technological University, Block N4.1, 50 Nanyang Avenue, Singapore 639798, Singapore

Introduction

Ni-free Cr–Mn–N stainless steels have been used as substitutes for common Cr–Ni grades because of their biocompatibility, superior mechanical features, good corrosion properties, and low costs [1–6]. Generally, these grades are produced by complex liquid state processes, such as pressurized electro-slag remelting under the high pressure of nitrogen [1–3, 6]; however, the nitrogen solubility in the liquid phase is limited due to nitride formation. Recently, solid-state processes like mechanical alloying (MA) have been regarded as an alternative route to produce these alloys [5–10].

During MA, powder particles are subjected to severe plastic deformation, repeated fracture, and cold welding, which promote extensive atomic scale alloying well beyond the equilibrium levels predicted by thermodynamics [11–14]. The generation of the high density of defects, especially dislocations and grain boundaries, may cause the material to become thermodynamically unstable, resulting in abnormal phase transformation [15, 16]. Consequently, the non-equilibrium states, including nanocrystals, amorphous phases, and supersaturated solid solutions can become stable during MA [11, 12, 17–20].

Recently, MA under the reactive nitrogen gas atmosphere has been used to synthesize the nanocrystalline [6–9, 21–24] and amorphous phases [25–30] through the solid–gas reaction. In case of Fe-based alloys, various

reports are available in the literature, among which are noticeable contributions by Rawers et al. [21–23] and Cisneros et al. [6–9]. The latter research group studied the influence of milling time, nitrogen levels, and annealing temperature on the volume fractions of the various crystalline phases (γ, α, Cr_2N, and CrN) in the high-nitrogen 18Cr11Mn and 18Cr11Mn5Mo stainless steels. It would be worth mentioning that the nanocrystalline phase quantification and characterization have taken the first priority in the aforementioned researches, whereas rarely have scientific efforts been conducted on the measurement and analysis of the amorphous phase which can be produced during MA. In this study, the quantitative and microscopic phase analyses as well as the thermal behavior of the nanocrystalline/amorphous Fe–18Cr–8Mn–xN powders synthesized by mechanically alloying have been studied.

Experimental procedure

The high-purity elemental powder, including Fe (>99.5%, $D_{av.} = 50$ μm), Cr (>99.9%, $D_{av.} = 150$ μm), and Mn (>99.9%, $D_{av.} = 50$ μm) supplied by Merck with a nominal composition of 74Fe–18Cr–8Mn (wt%) were used as the primary materials. MA was performed in the Iran Mahand high-energy shaker mill with a tempered steel bowl (Capacity = 150 mL) at a rotation speed of 400 rpm. Four tempered steel balls of 20-mm and seven tempered steel balls of 8-mm diameters giving a ball:powder mass ratio of 10:1 were used. Samples were obtained at different milling times at 24-h intervals up to 144 h. The milling process was conducted under a continuous flow (10 mL/min) of high-purity N_2 gas (>99.999%) using an accurate flow controller. A positive pressure was maintained in the milling chamber by placing the gas outlet tube under 100 mm water. To consider the effect of nitrogen on the phase transformation during MA, the ball milling process was also performed under an inert gas (high-purity Ar gas) atmosphere by the same procedure.

The total N, O, and C contents of the powder samples were measured using LECO TC 436 and CS 600 (Leco Corp., St. Joseph, MI) systems. The Fe, Cr, and Mn contents were determined by an X-ray fluorescence analyzer (Philips PW2400). In this test, the quantitative values were extracted by the PAN analytical software. The structural phase analysis was conducted by the Shimadzu lab X-6000 X-ray diffractometer using Cu $K\alpha_{1,2}$ radiation and the secondary curved graphite monochromator. For all the investigations, the angular range (2θ) of 30 to 100° with a step width of 0.02 and a step time of 3 s was used. The X-ray tube was operated at 40 kV and 40 mA. The quantitative analysis of the X-ray diffraction (XRD) data was performed by TOPAS 3 from Bruker AXS. Using this software, the relative content of the available phases was estimated by the Rietveld method and the average crystallite size of the crystalline phases was determined by the Double-Voigt approach. The amorphous phase content was also determined by Rietveld analyzing the XRD pattern of a mixture of the as-milled powders and the known amount of nanocrystalline Fe powder as a standard. The powder:standard weight ratio of 75:25 was used for this purpose. To investigate the microstructural features of the as-milled powders and to confirm the crystallite sizes obtained from XRD, selected powder particles were dispersed in ethanol, dropped down to a copper grid, and then characterized by a high-resolution transmission electron microscope (TEM, JEOL-JEM 2010) in the bright-field and high-resolution modes. The crystallite size measurements were performed on each sample at ten different locations to increase the test accuracy. The thermal stability of the alloyed powders was investigated by differential scanning calorimetry (DTA/DSC, NETZSCH, STA 449C Jupiter) with an alumina container under a flowing purified argon gas atmosphere. Prior to analysis, the pellet samples with an approximate diameter of 5 mm were prepared by a uniaxial compression method and used as an initial material for the DSC test.

Results

Chemical composition assessment

Table 1 lists the chemical composition of the samples obtained at various milling times. It is obvious that the expected nominal composition of 18 wt% Cr + 8 wt% Mn was achieved and the only detectable impurity in the as-milled powders is oxygen which belongs to the natural oxidation of the powders in the atmosphere. For the samples milled under the nitrogen gas atmosphere, the nitrogen content has risen by increasing the milling time to 2.54 wt% after 144 h. This implies that during MA under the nitrogen atmosphere as a consequence of solid–gas reactions the high quantity of nitrogen atoms will diffuse into the structure of the alloyed powders.

Microstructural evaluation

XRD analysis

Figures 1 and 2 show the XRD patterns of the mechanically alloyed powders milled under the nitrogen and argon gas atmospheres, respectively. It is clear that for the samples milled under the nitrogen gas atmosphere, the dominant crystalline phase at short milling times is ferrite (α) in which the peak intensity steadily fades by increasing

Table 1 Chemical composition of the as-milled powders

Milling atmosphere	Milling time (h)	Weight percent (wt%)											
		Fe		Cr		Mn		N		O		C	
		Con	AE	Con	AE	Con	AE	Con	AE	Con	AE	Con	AE
N_2	24	72.978	0.080	17.748	0.050	8.225	0.030	0.693	0.005	0.325	0.004	0.032	0.002
	48	72.948	0.090	17.643	0.040	8.069	0.020	0.973	0.007	0.334	0.005	0.033	0.001
	72	72.971	0.070	17.505	0.050	7.827	0.030	1.330	0.009	0.334	0.005	0.033	0.001
	96	72.763	0.080	17.408	0.040	7.705	0.020	1.760	0.012	0.335	0.006	0.029	0.002
	120	72.530	0.090	17.350	0.050	7.629	0.030	2.130	0.016	0.331	0.004	0.030	0.001
	144	72.319	0.080	17.203	0.040	7.576	0.030	2.537	0.019	0.334	0.005	0.031	0.002
Ar	24	73.524	0.090	17.941	0.050	8.120	0.020	0.041	0.002	0.341	0.005	0.033	0.002
	48	73.790	0.090	17.812	0.040	8.012	0.030	0.032	0.002	0.323	0.005	0.031	0.001
	72	74.242	0.100	17.631	0.050	7.710	0.030	0.043	0.002	0.344	0.004	0.030	0.001
	96	74.379	0.090	17.542	0.040	7.662	0.030	0.039	0.001	0.347	0.005	0.031	0.002
	120	74.586	0.080	17.412	0.050	7.604	0.020	0.032	0.002	0.334	0.005	0.032	0.002
	144	74.719	0.070	17.343	0.050	7.531	0.030	0.034	0.001	0.340	0.004	0.033	0.002

Con concentration, *AE* absolute error

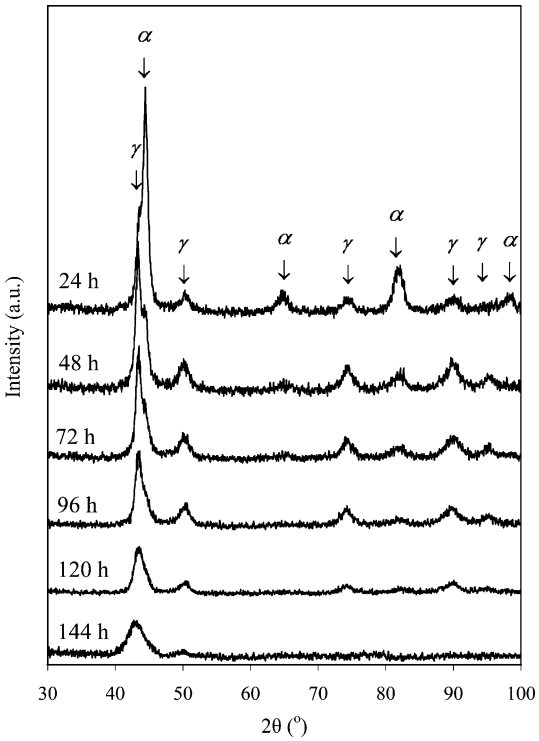

Fig. 1 The XRD pattern of the powders milled under nitrogen

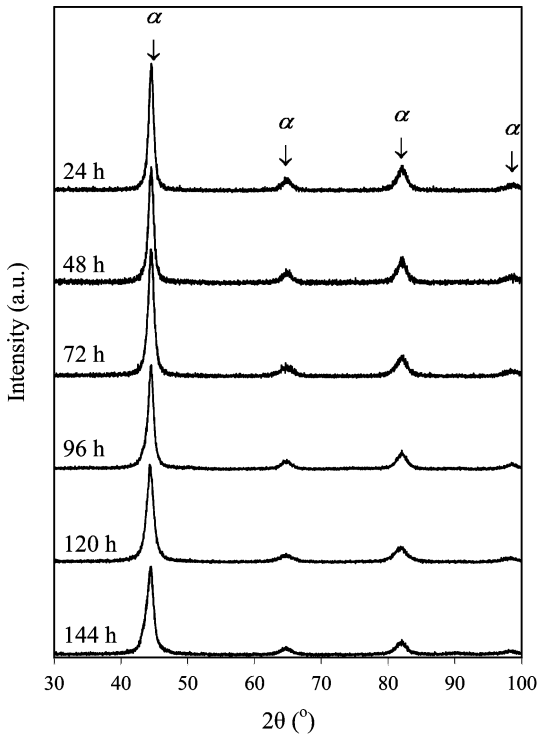

Fig. 2 The XRD pattern of the powders milled under argon

the milling time as the austenite (γ) peaks become dominant (Fig. 1). In contrast, milling under the argon atmosphere does not lead to any detectable structural changes and the structure of all grades contains the predominant crystalline α-phase (Fig. 2). Table 2 lists the variation of austenite and ferrite phase contents in the crystalline structure after the different milling intervals. As it is obvious, in the samples milled under the nitrogen gas atmosphere, the quantity of austenite phase increases by increasing the milling time and becomes dominant after 48 h of milling. On the contrary, the quantity of crystalline austenite phase in the structure of the alloyed powders milled under the argon atmosphere is quite low. It reveals that the high-energy ball milling of the elemental Fe, Cr, and Mn powders under the nitrogen gas atmosphere has resulted in the structural transformation of bcc to fcc

Table 2 The quantity variation of austenite and ferrite in the crystalline phase

Milling time (h)	Crystalline phase content (wt%)			
	Nitrogen atmosphere		Argon atmosphere	
	Ferrite (α)	Austenite (γ)	Ferrite (α)	Austenite (γ)
24	72.8 <4>	27.2 <4>	98.6 <3>	1.4 <3>
48	37.8 <3>	62.2 <3>	98.3 <3>	1.7 <3>
72	31.4 <4>	68.6 <4>	98.2 <4>	1.8 <4>
96	25.7 <2>	74.3 <2>	97.9 <3>	2.1 <3>
120	16.4 <3>	83.6 <3>	97.7 <4>	2.3 <4>
144	8.6 <2>	91.4 <2>	97.6 <3>	2.4 <3>

Error value: $<X> \equiv \pm 0.X$ wt%

through the dissolution of Cr, Mn, and N in the solid solution. It also signifies that the milling atmosphere acts as an important role in the α-to-γ phase transformation during MA. Figure 3 represents the crystallite size variation of austenite and ferrite phases as a function of the milling time. Noted that the crystallite size of austenite in the samples milled under the argon atmosphere could not be measured due to the low amount of austenite in the structure and the overlapping of the concerned major peaks of ferrite and austenite. According to this figure, it can be seen that the crystallite size of the present phases is at the nanomeric levels and decreases by increasing the milling time. The results show that the grain refinement under the nitrogen atmosphere occurs more significantly and more rapidly than the argon atmosphere. Consequently, it can be inferred that the incorporation of nitrogen into the structure during milling has a considerable effect on the crystallite size of the crystalline phases.

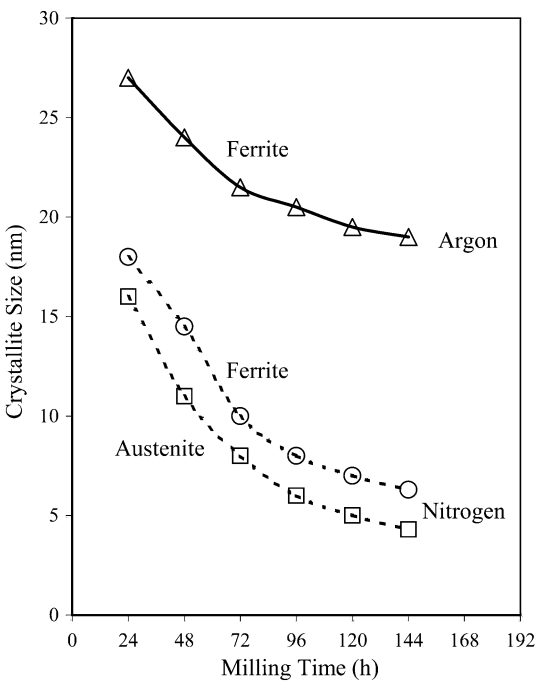

Fig. 3 The crystallite size variation of the austenite and ferrite phases measured by XRD

More focus on the XRD results of Figs. 1 and 2 signifies that by progression of the MA process the broadening of the XRD peaks is increased. This phenomenon can be due to the decrease in the crystallite size, the increase in the lattice strain, and/or the existence of the amorphous phase in the structure. In the case of milling under the nitrogen atmosphere (Fig. 1), unlike the argon atmosphere, by increasing the milling time the broadening of the first-order peaks corresponding to the (111) and (110) reflections in the fcc and bcc structures, respectively, is increased considerably and the peaks related to higher-order reflections ($2\theta > 50°$) are beginning to disappear. In these samples, at sufficiently high milling times (e.g., 144 h), the XRD pattern becomes hallo. This can be due to the existence of a high amount of amorphous phase in the structure. However, the presence of the detectable intensity peak correlated with (200) reflection in the XRD pattern indicates that a noticeable amount of crystalline phases is available in the microstructure.

In order to determine the proportion of amorphous phase in the as-milled powder samples, the method proposed by Winburn et al. [31] based on the Rietveld quantitative analysis was used. The method derives the amorphous phase content from the overestimation of an internal crystalline standard in the Rietveld refinement of an appropriate mixture of standard and the sample powders [32–35]. The nanocrystalline Fe powder with an average crystallite size of 20 nm, prepared by ball milling of pure Fe (>99.5%) under the argon atmosphere for 1 h, was used as the standard. To ensure that the standard itself was free from the amorphous phase, DSC (NETZSCH, STA 449C Jupiter) was performed on the above-mentioned standard material thrice and no amorphous-to-crystalline transformation was detected at different heating rates (10, 20, and 50 °C/min). New powder mixtures were made by mixing the 75 wt% of the as-milled alloy powders with 25 wt% of the standard. Prior to mixing, the sieving process was performed on the as-milled and standard powders separately, and particles smaller than 38 μm were used for quantitative analysis. For a reliable amorphous phase analysis, reproducible Rietveld refinements with low-phase fraction deviations are required. The XRD data collections and their quantitative Rietveld analyses were repeated thrice in three specimens to check for repeatability and to estimate the potential errors. De La Torre et al. [32] proposed Eq. 1 for the weight percentage of the amorphous phase identified by A in a sample that contains a mixture of amorphous and a known crystalline phase (the standard, in our case).

$$A = \frac{1 - (W_S/R_S)}{100 - W_S} \times 10^4\%, \quad (1)$$

where W_S (%) is the weight concentration of the internal standard (in this study $W_S = 25\%$) and R_S (%) is its Rietveld analyzed concentration (RAC). In this study, since the structure of Fe (α) standard is similar to the crystalline phases in the alloy powders, R_S can be replaced by the modified RAC (MRAC), which can be easily derived using Eq. 2.

$$R_{S(Fe)} = W_{R(\alpha)} - X \times W_{(\gamma)}, \quad (2)$$

where $R_{S(Fe)}$ is the MRAC of Fe standard and $W_{R(\gamma)}$ and $W_{R(\alpha)}$ are RACs of austenite and ferrite (after mixing with the standard), respectively. The quantity X is the Rietveld weight ratio of ferrite to austenite in the as-milled alloy powder. Equation 2 is based on the fact that the weight ratio of crystalline phases in the as-milled powder is independent of the amorphous phase content and does not vary when the standard is added. According to the above-mentioned procedure, the amorphous phase content of the samples milled under both nitrogen and argon gas atmospheres was estimated. Because of further clarity, the calculation details of the amorphous phase content (A) in the samples milled under the nitrogen atmosphere are listed in Table 3.

With regard to the amorphous phase content in the as-milled powders and the austenite and ferrite phase contents in the crystalline structure (Table 2), the relative α, γ, and amorphous phase contents of the powders can be determined. Table 4 represents the variation of each phase with the milling time. It can explicitly be observed that, in the samples milled under nitrogen, the proportion of the amorphous phase is considerably high and, as expected, rises by increasing the milling time and becomes dominant after 72 h. On the contrary, in the samples milled under the argon atmosphere, the dominant phase is the crystalline α phase and the quantity of amorphous phase is rather low and does not change considerably by progression of MA. Therefore, in the present case, it can be inferred that the infused nitrogen has the main contribution to the amorphization process during MA. Table 4 also shows that in the samples milled under the nitrogen atmosphere, the percentage of austenite increases and then, due to the continuous increase in the percentage of amorphous phase, begins to decrease. Apparently, there exists a competition between the amorphization process and the austenite

Table 3 The calculation details of the amorphous phase content

Milling time (h)	Weight percent of phases									
	As-milled alloy			After mixing with Fe						Approximate amorphous content (A)
	$W_{R(\gamma)}$	$W_{R(\alpha)}$	X	Specimen 1		Specimen 2		Specimen 3		
				$W_{R(\gamma)}$	$W_{R(\alpha)}$	$W_{R(\gamma)}$	$W_{R(\alpha)}$	$W_{R(\gamma)}$	$W_{R(\alpha)}$	
24	27.2	72.8	2.7	18.51	81.49	18.53	81.47	18.49	81.51	29.0
48	62.2	37.8	0.6	40.14	59.86	40.11	59.89	40.19	59.81	39.3
72	68.6	31.4	0.5	43.11	56.89	43.13	56.87	42.99	57.01	43.7
96	74.3	25.7	0.3	42.91	57.09	42.97	57.03	42.93	57.07	54.4
120	83.6	16.4	0.2	41.33	58.67	41.25	58.75	41.47	58.53	67.4
144	91.4	8.6	0.1	30.04	69.96	29.92	70.08	30.21	69.79	83.7

Table 4 The relative phase content of the as-milled powders

Milling time (h)	Relative Phase Content (wt%)					
	Nitrogen Atmosphere			Argon Atmosphere		
	Amorphous phase	Austenite (γ)	Ferrite (α)	Amorphous phase	Austenite (γ)	Ferrite (α)
24	29.0 <3>	19.3 <4>	51.7 <4>	1.5 <3>	1.4 <3>	97.1 <3>
48	39.3 <2>	37.8 <3>	22.9 <3>	1.9 <4>	1.6 <3>	96.5 <3>
72	43.7 <4>	38.6 <4>	17.7 <4>	2.2 <2>	1.7 <4>	96.1 <4>
96	54.4 <2>	33.9 <2>	11.7 <2>	2.5 <3>	2.0 <3>	95.5 <3>
120	67.4 <3>	27.3 <3>	5.3 <3>	2.8 <2>	2.2 <4>	95.0 <4>
144	83.7 <2>	14.9 <2>	1.4 <2>	3.2 <2>	2.3 <3>	94.5 <3>

Error value: $<X> \equiv \pm 0.X$ wt%

formation during MA in such a way that the amorphization overcomes the austenite formation after 72 h of milling.

TEM observations

In order to identify the exact available phases and to confirm the crystallite sizes obtained from XRD, microscopic studies were conducted on selected powder particles by TEM. The crystallite size measurements were performed on the samples milled for 48 and 96 h. To facilitate the crystallite size measurement, the crystallite type (ferrite or austenite) was not taken into consideration. Table 5 shows the results of the crystallite size measurement. These results are compatible with those of Fig. 3, indicating the reliability of the XRD results. The phase identification was made on the samples milled for 144 h. Figure 4a shows the bright field TEM images of a powder particle after 144 h milling under the nitrogen atmosphere. The image can clearly be separated into two sections—the dark regions with the average size of 50 nm and the bright matrix. This difference in the TEM contrast could originate from the orientation variations (Bragg contrast), mass-thickness differences, or dual-phase structure. In order to determine the basis of these regions, a high-resolution image and the corresponding selected area diffraction (SAD) pattern were obtained from the dark and bright sections separately (Fig. 4b, c). The results reveal that the dark regions are a combination of the nanocrystalline austenite and ferrite phases and the bright matrix is a featureless amorphous phase, i.e., the microstructure is composed of the amorphous and nanocrystalline phases. As it can be seen, the amorphous phase content is substantially high, confirming the quantitative analysis of the XRD data. Figure 5 shows the high-resolution image and the SAD pattern of the powder milled under the argon gas atmosphere for 144 h. This reveals that the structure contains a predominant nanocrystalline α-phase. By comparing the image of Figs. 4 and 5, it can be concluded that the milling atmosphere plays an essential role in the α-to-γ phase transformation and the amorphization during MA of the powders.

Table 5 The crystallite size of the crystalline phases measured by TEM

Milling atmosphere	Milling time (h)	Crystallite size (nm)	
		Minimum	Maximum
Nitrogen	48	9	17
	96	5	11
Argon	48	18	28
	96	15	22

DSC studies

In order to study the thermal behavior of the as-milled powders, the DSC test was used at a constant heating rate of 10 K/min. All the samples were heated up to 900 K (first run) and cooled down to about 400 K. Then, the second heating runs were performed to establish the base line. Figure 6 shows the DSC results of the samples milled under the nitrogen gas atmospheres. It reveals the two exothermic peaks appearing around 660 and 840 K, respectively. In order to determine the origin of these reactions, the DSC test was performed again on the as-milled samples in the same manner and the samples were

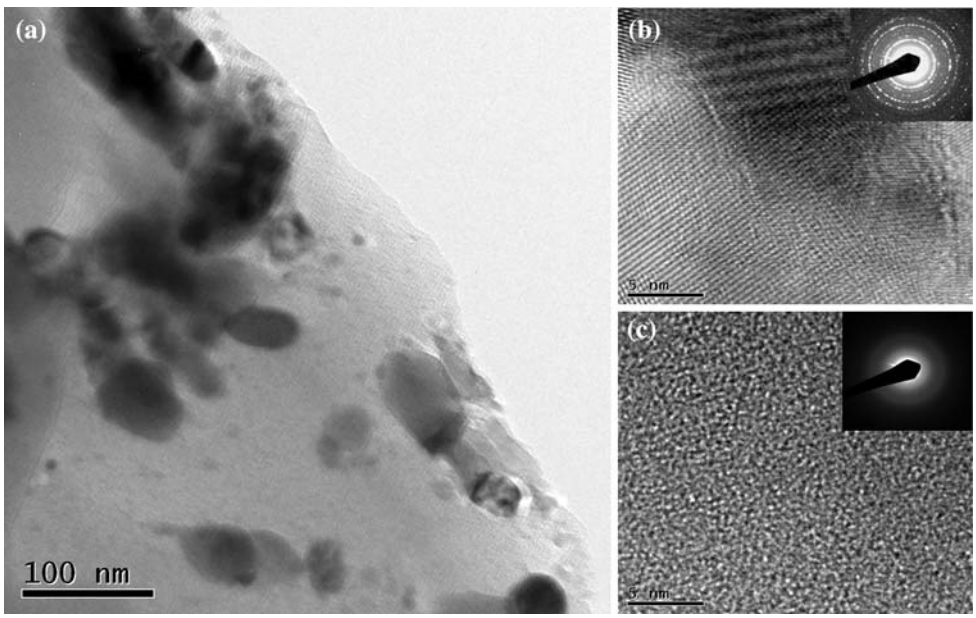

Fig. 4 The TEM micrograph of the powder milled under nitrogen after 144 h. **a** Bright field image; **b** high-resolution image with correlated SAD pattern of the dark regions of (**a**); **c** high-resolution image with corresponding SAD pattern of the bright matrix of (**a**)

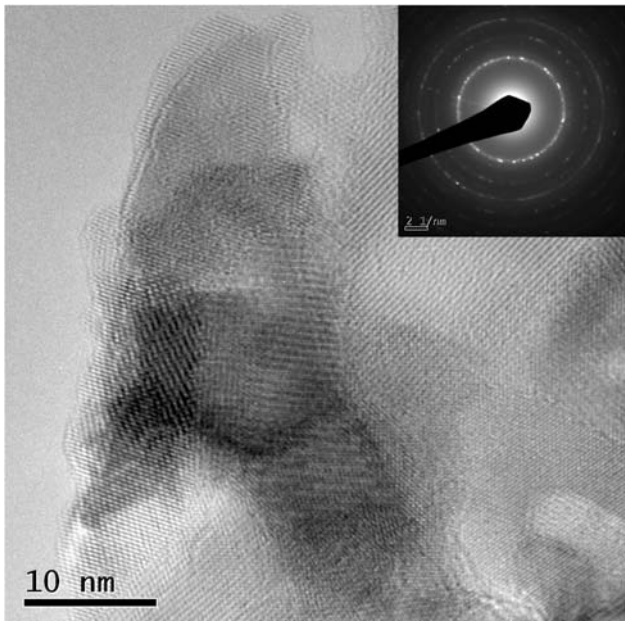

Fig. 5 The HRTEM image of the powder milled under argon for 144 h

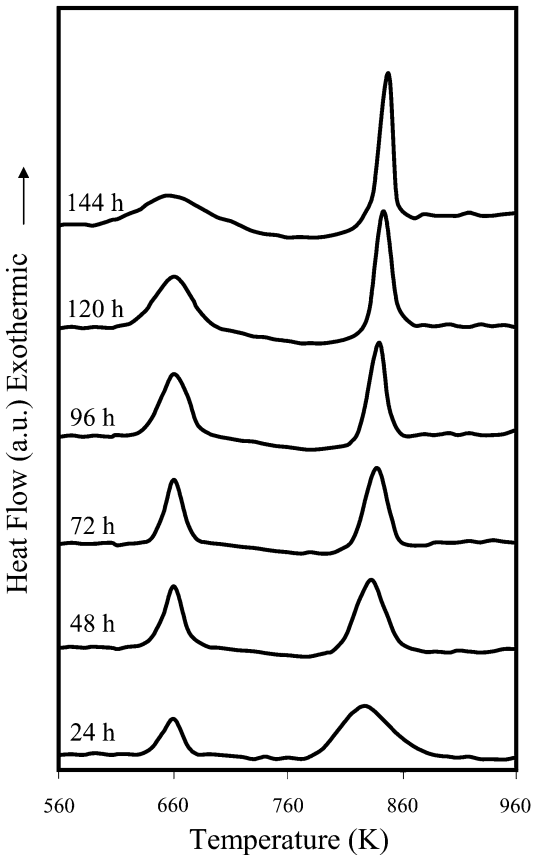

Fig. 6 The DSC profile of the samples milled under nitrogen at constant heating rate of 10 K/min

heated up to the temperatures well below and above the temperature ranges of the reactions. Subsequently, the XRD analyses were performed on these samples at room

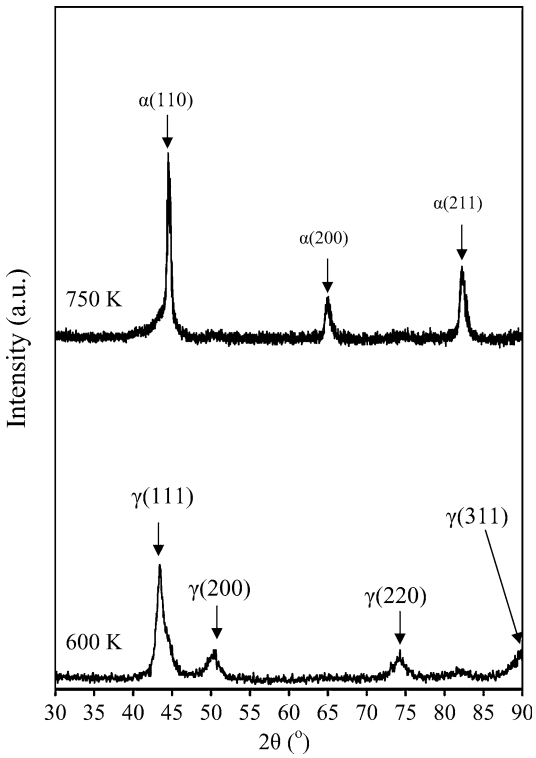

Fig. 7 The XRD pattern of the sample milled under nitrogen for 96 h after DSC test at 600 and 750 K

temperature. Figures 7 and 8 depict the XRD pattern of the samples milled under the nitrogen atmosphere for 96 and 144 h, respectively, after DSC test. Comparing the DSC results (Fig. 6) and the XRD pattern (Figs. 7 and 8) indicated that the first exothermic peak in the DSC curve corresponds to the structural transformation of γ-phase to α-phase and the second one is related to crystallization of the amorphous phase and the formation of a crystalline ferrite and the CrN and Cr_2N phases. By the progression of the MA process, the intensity of the first peak in the DSC curve of Fig. 6 increases and then decreases. This is compatible with the quantitative XRD results of Table 4. Moreover, by increasing the milling time, the second peak (the crystallization peak) moves to the high-temperature side, becoming sharper and more pronounced. This reveals that the amorphous phase quantity and homogeneity increase by progression of the MA process. In order to distinguish the crystallization of the amorphous phase with the grain growth phenomenon of a nanocrystalline material, the isothermal DSC was performed on the sample that was milled for 144 h at 800 K (Fig. 9). The signals exhibit the typical bell-shape for the first-order phase transition associated with the nucleation and growth phenomena. This confirms unambiguously that the high-temperature exothermic peak as shown in Fig. 6 is related to the crystallization of the amorphous phase.

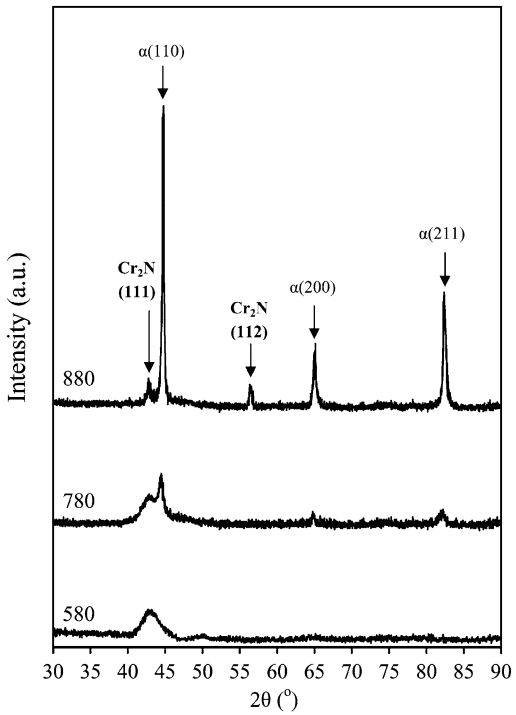

Fig. 8 The XRD pattern of the sample milled under nitrogen for 144 h after DSC test at 580, 780, and 880 K

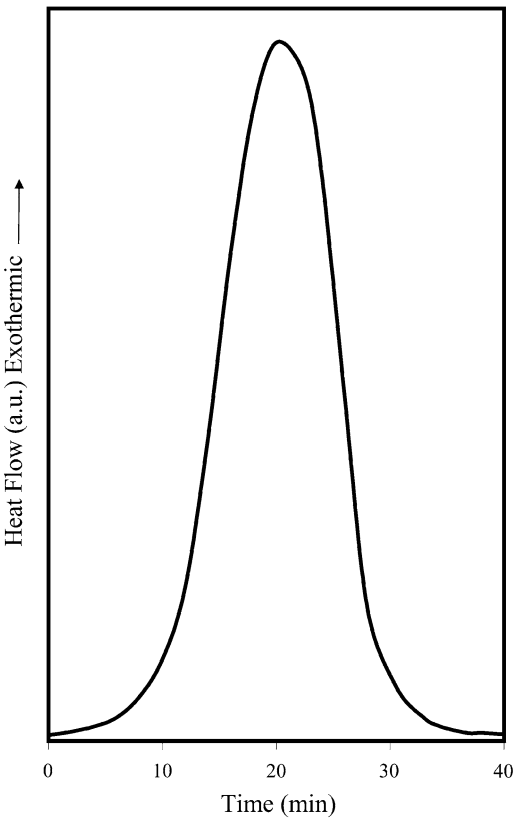

Fig. 9 The isothermal DSC test of the sample milled under nitrogen for 144 h

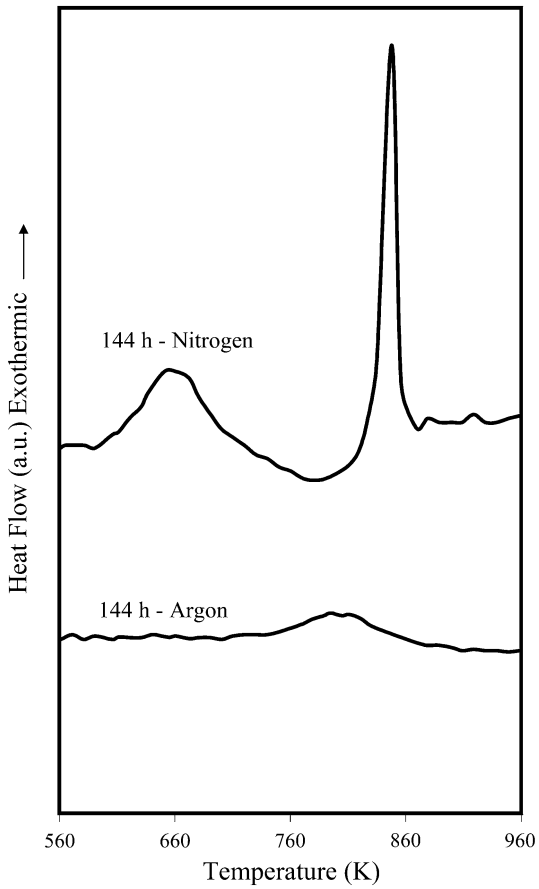

Fig. 10 Comparing the DSC profile of the samples milled for 144 h under the nitrogen and argon atmospheres

Figure 10 compares the DSC results of the powders milled for 144 h under the argon and nitrogen gas atmospheres. As can be seen, in contrast to the samples milled under the nitrogen atmosphere, the DSC trace of those milled under the argon atmosphere contains simply one broad exothermic event corresponding to the crystallization of the amorphous phase which is available in a small amount along with the crystalline phases. In this case, as the amount of austenite phase in the as-milled powders is very low, the γ-to-α phase transformation peak is not detectable in the DSC trace.

According to the above-mentioned results, it can be concluded that without using nitrogen as the milling atmosphere, the α-to-γ phase transformation and the amorphization process are diminished dramatically during the milling process.

Discussion

MA of the elemental powder mixtures with the nominal composition of Fe–18Cr–8Mn under the nitrogen gas atmosphere has resulted in the infusion of a high proportion

of nitrogen atoms into the structure and extreme disordering, leading to the α-to-γ phase transformation and the amorphization of the powders. The infused nitrogen also improves the thermal stability of the amorphous phase and enhances the grain refinement phenomenon during MA. The contribution of the dissolved nitrogen atoms to these phenomena is discussed in the following sections.

Nitrogen incorporation

When milling is performed under the nitrogen atmosphere, nitrogen is adsorbed on the newly created surfaces of the powder particles and penetrates into the structure by diffusing down to the interstitial sites of crystallite, grain boundaries, dislocations, and other defects. Since the amount of structural defects generated by the severe plastic deformation during milling is rather high, and since the mismatch strain of the solute nitrogen can be reduced in the grain boundaries and the elastic field of dislocations, a high proportion of nitrogen atoms are diffused down to the dislocations and grain boundaries [25]. Thus, the contribution of the dislocations and grain boundaries to the nitrogen dissolution is considerably high.

Grain refinement

In the "Results" section, it was shown that the milling process under both nitrogen and argon atmospheres develops the nano-size structures even at low milling times (e.g., 25 h). It was also found out that in the samples milled under the nitrogen atmosphere, the grain refinement occurs more rapidly and more significantly than the samples milled under the argon atmosphere. These trends are to be discussed below.

During MA, the powder particles are subjected to the severe plastic deformation and extreme cold working. Under these conditions, the dislocation density increases to considerably high levels and the shear bands containing a high dislocation density are formed in the structure. With continued milling, the lattice strain increases by increasing the dislocation density, leading to the formation of dislocation cells and the subgrains separated by low-angle grain boundaries (recovery). After sufficient milling times, the transformation of the low-angle grain boundaries into those of the high-angle takes place by grain rotation. The grain refinement continues until a balance is established between the hardening process caused by plastic deformation and the recovery process due to the annihilation and arrangement of dislocations [14, 36]. When milling is performed under the nitrogen atmosphere, a high percentage of nitrogen atoms can infuse into the structure by diffusing down to the dislocations and the grain boundaries. The diffused nitrogen atoms will be segregated into the dislocations and the grain boundaries. This phenomenon contributes to the fixing of the dislocations and the stabilizing of the grain boundaries [25]. Afterwards the trickling down of the running dislocations on the fixed dislocations leads to the nucleation of new boundaries [37]. This results in rapid grain refinement in the order of a few nanometers, compared with the powders milled under the argon atmosphere. It would be worth mentioning that at every step of the milling process, the crystallite size of the samples milled under nitrogen is less than that of the samples milled under argon. This indicates that the infused nitrogen atoms play a considerable role in decreasing the minimum grain size ($d_{\min}$) achievable by mechanical milling. Mohamed [38] proposed a dislocation model to estimate the value of $d_{\min}$ during the milling process. This model is in agreement with the experimental data of other researchers [39, 40]. According to this model, the normalized minimum grain size ($d_{\min}/b$) obtainable by milling is related to the different structural properties, such as hardness (H), self-diffusion activation energy (Q), stacking fault energy (SFE) (γ), shear modulus (G), and milling temperature (T) as follows:

$$d_{\min}/b \propto (e^{-\beta Q/4RT})(1/T)^{0.25}(G)(\gamma)^{0.5}(1/H)^{1.25}, \quad (3)$$

where b, R, and β are the Burgers vector, the gas constant, and a constant less than unity, respectively. The term "βQ" is the activation energy for the recovery process. To describe the effect of the dissolved nitrogen atoms on $d_{\min}/b$, the variations of the above-mentioned parameters with the nitrogen concentration have been considered below.

Nitrogen versus the activation energy

According to Eq. 3, the self-diffusion activation energy is one of the parameters affecting $d_{\min}$. At the high activation energy, the rate of recovery is very low; as a result, $d_{\min}/b$ is decreased. It has been shown that Q is proportional to an appropriate elastic modulus (E) and the cube of the lattice parameter (a^3) according to the following equation [41]:

$$Q = cEa^3, \quad (4)$$

where c is a constant. In addition, Q scales with the melting temperature (T_m) as follows [42]:

$$Q \sim \lambda RT_m, \quad (5)$$

where λ is about 17.5. To determine the effect of the dissolved nitrogen on Q, the nitrogen effect on a, E, T_m has been evaluated as follows.

The interstitial dissolution of the nitrogen atoms expands the lattice and consequently increases the lattice parameter. On the other hand, the value of E decreases by the infusion of nitrogen atoms into the structure of stainless steels [43, 44]. Furthermore, since the dissolved nitrogen atoms form a strong bonding with the constituent elements

(especially Cr) and increase the lattice strain, the melting temperature is increased by increasing the amount of nitrogen [45]. On the basis of these facts and according to Eqs. 4 and 5, the competition between a^3, E, and T_m determines the variations of Q with nitrogen. If a^3 and T_m dominate over E, the value of Q will increase by the nitrogen infusion. However, in reverse (i.e., the dominating of E over a^3 and T_m), the value of Q will decrease by the nitrogen infusion. Considering just the effect of Q on d_{min}, the quantity of d_{min}/b will decrease by increasing the amount of Q, being compatible with the experimental results given in this study. In contrast, in case of the decreasing of the Q value by increasing the nitrogen level, the effect of this parameter (Q) on d_{min}/b, compared with the other terms of Eq. 3, will be less significant.

Nitrogen versus the SFE

To the best of our knowledge, most of the investigations focused on the effect of nitrogen on the SFE of fcc steels and there is no attempt on bcc steels. In the present case, as the dominant crystalline phase at high milling times is austenite, the effect of nitrogen on SFE of austenite is discussed. There exist different approaches in the literature regarding the effect of nitrogen on SFE of austenitic steels. Several researchers have reported that the addition of nitrogen results in a decrease in SFE of austenitic steels [46–48]. In contrast to these results, other studies have found that the dissolved nitrogen increases SFE of fcc iron-based alloys [49, 50]. Finally, some studies have indicated that SFE of austenitic stainless steels depends non-monotonically on the nitrogen content [51]. Yakubtsovi et al. [52] represented the two contributions to SFE which arises from the bulk of the alloy due to the nitrogen addition ($\eta_{(b)N}$) and the segregation of nitrogen into the stacking faults ($\eta_{(s)N}$). They also showed that nitrogen increases the $\eta_{(b)N}$ values while it decreases the $\eta_{(s)N}$ values of the system. Recently, Gavriljuk et al. [53] have found that in the nickel-free Cr–Mn austenitic stainless steels, SFE decreases by increasing nitrogen and then increases when the nitrogen concentration increases up to 0.8 wt%. This is compatible with Yakubtsovi's hypothesis. The initial decrease in SFE is due to the segregation of impurity atoms into the dislocations and the second increase is due to the overcoming of the bulk effect over the segregation effect. In the present case, when milling performed under the nitrogen atmosphere, due to the severe plastic deformation, the dislocation density in the structure increases to very high levels and due to the development of the nano-size structure, the proportion of the metal atoms presented in the grain boundaries increases significantly. On the other hand, as discussed before, a high percentage of the infused nitrogen was segregated into the dislocations and grain boundaries. Consequently, it can be inferred that the contribution of $\eta_{(s)N}$ to the SFE is considerable and by increasing the dissolved nitrogen the SFE decreases. According to Eq. 3, $(\gamma)^{0.5}$ scales directly with d_{min}/b, indicating that the value of d_{min}/b decreases by the nitrogen incorporation, provided that just the effect of SFE on d_{min} is considered.

Nitrogen versus the hardness and the shear modulus

It is well established that nitrogen increases the strength and hardness of stainless steels by the solid solution and grain size (Hall-Petch) strengthening [54, 55]. In addition, by the dissolution of nitrogen atoms the lattice is expanded and the volume increases; consequently, the shear modulus decreases [43, 44]. According to the literature [39], another important factor affecting d_{min} is the minimum dislocation separation in a pile-up (L), which is in direct proportion to d_{min}. This parameter is in direct relation to the shear modulus and is in inverse proportion to the hardness as follows [39, 56]:

$$L = 3G\mathbf{b}/\pi(1-\nu)H, \tag{6}$$

where $\mathbf{b}$ is Burgers vector and ν is Poisson's ratio. As the infusion of nitrogen increases the hardness and decreases the shear modulus, the equilibrium distance between two edge dislocations decreases. Based on these details and according to Eq. 3, it can be inferred that the amount of d_{min}/b decreases by increasing the dissolved nitrogen, providing that just the effects of G, H, and L on d_{min} are taken into consideration.

Based on the entire afore-mentioned effect of nitrogen on the structural properties, it can be concluded that the further grain refinement of the samples milled under the nitrogen atmosphere, compared with those milled under the argon atmosphere, is explained by the effect of the dissolved nitrogen on the minimum achievable grain size during milling.

Phase transformation

Amorphization

In the "Results" section, it was found that the dissolved nitrogen atoms infused during milling under the nitrogen atmosphere play an essential role in the amorphization process. There exist different approaches to the amorphization process. Most of them were developed for the materials prepared by rapid quenching, vapor deposition, or MA [25–27, 57, 58]. In this study, it is recognized that the atomic-size, heat-of-mixing, and extreme structural refinement effects are the main causes of the amorphization as described below.

Atomic size effect During MA, due to the atomic size differences, the dissolution of the alloying elements inside the substitutional and interstitial sites of crystallite and grain boundaries of the host material can dilate the crystal to increase the lattice strain and consequently increase the internal energy of the system. Egami and Waseda [57] suggested that solid solutions become unstable above a certain solute concentration (C_B^{min}). They developed the following relationship between C_B^{min} and the atomic volume mismatch $|(V_B - V_A)/V_A|$ for binary alloy systems:

$$C_B^{min} \approx |\frac{V_A}{V_B - V_A}| \times 0.1, \quad (7)$$

where V is the atomic volume of specific atoms. In the present case, as the atomic size difference among Fe, Cr, and Mn is low, in the absence of any other solute source the volume mismatch is not considerable and consequently C_B^{min} is quite high. According to the "Results" section, no phase change was detected in the samples milled under the argon atmosphere. That is, the present solute contents (18 wt% Cr and 8 wt% Mn) are not sufficient for instability and phase transformation. When milling is performed under the nitrogen atmosphere, the nitrogen atoms can infuse into the structure and act as the main source of the mismatch strain. Rawers et al. [23] reported that the incorporation of 4 wt% nitrogen can change the lattice strain of the as-milled powders from 0.5 (for the powders processed in the argon atmosphere) to 1.3.% (for the powders processed in the nitrogen atmosphere). In the samples milled under the nitrogen atmosphere, at the early stage of milling, the α-phase is the predominant crystalline phase, which becomes unstable by increasing the dissolved nitrogen concentration. Consequently, the mismatch strain and the internal energy of the system increase. Under these conditions, the α-phase will be transformed into the more stable phases. Since the atomic size effect is less in the amorphous phase than the grain boundary and is less in the grain boundary than the crystalline lattice [25], from this point of view, the thermodynamic stability of the amorphous phase is higher than the grain boundary and that of the grain boundary is higher than the crystallite. This reveals that for the progressive dissolution of the nitrogen atoms in the structure, the grain refinement and subsequently the amorphization are required. At a sufficiently high concentration of the nitrogen atoms, the amorphous phase will initiate along grain boundaries and consume the crystalline lattice unless more stable phases like nitrides nucleate [25].

Heat of mixing considerations It is demonstrated that the effect of the atomic size alone is not sufficient to describe the amorphization process and in addition to the aforementioned reason, intermixing at atomic levels is the other important cause of amorphization. It was reported that the intermixing of the constituent elements of iron and nitrogen does not fully occur on an atomic scale during MA and other constituents like chromium and manganese are essential to the achievement of a fully amorphized structure [27]. Accordingly, it seems that when Cr and Mn with high affinity for N are added to Fe–N alloys, the intermixing of the atomic species Fe, Cr, Mn, and N readily occurs at atomic levels, resulting in the formation of the amorphous phase. In order to evaluate the effects of Cr and Mn on the amorphization of the Fe–N alloys thermodynamically, the values of the interaction parameters of Cr and Mn with N atoms (W_{Cr-N} and W_{Mn-N}) proposed by Miura et al. [27] were used. The interaction parameter represents the difference between the bonding energy of the Cr–N and Fe–N ($U_{Cr-N} - U_{Fe-N}$) atomic pairs and that of the Mn–N and Fe–N ($U_{Mn-N} - U_{Fe-N}$) pairs in the ternary Fe–Cr–N and Fe–Mn–N solutions, respectively. The quantities of W_{Cr-N} and W_{Mn-N} are negative but the absolute value of W_{Cr-N} is higher, which demonstrates the stronger interaction and bonding between Cr and N. With the negative interaction parameters, the mixing enthalpy of the system is negative [59] and the formation of the ternary Fe–Cr–N and Fe–Mn–N solutions results in decreasing the free energy of the system. In other words, the addition of such elements to the Fe–N alloy provides a thermodynamic driving force for the formation of the ternary solution, and the intermixing of the constituent atoms becomes easier. Another aspect of the negative heat of mixing is the decrease in the activity of nitrogen due to the strong interaction of Cr and Mn with N. This prohibits the diffusion of the nitrogen atoms over a large distance during MA, thereby retarding the nucleation and growth of the crystalline phases. This increases the possibility of the amorphous phase formation during MA [27].

Effect of extreme structural refinement As discussed above, the dissolved nitrogen atoms have a significant effect on the grain refinement. Ogino et al. [26] proposed that in the milling process, as a result of the grain refinement phenomenon, the constraints of the neighboring grains will increase and when the grain sizes are reduced in the order of few nanometers (possibly <5 nm), the crystallite becomes unstable, leading to the amorphization. Since in the samples milled under the nitrogen atmosphere, the average crystallite size of both austenite and ferrite phases is considerably less in the samples milled under nitrogen than argon, this effect can be an important factor in the amorphous phase formation during milling under nitrogen.

Ferrite to austenite phase transformation

According to the "Results" section, it can be seen that, in contrast to the samples milled under the argon atmosphere,

in the samples milled under the nitrogen atmosphere, the ferrite-to-austenite phase transformation can occur during MA. During MA under nitrogen, a proportion of nitrogen atoms can diffuse into the interstitial sites of the crystallite and produce the mismatch strains in the crystallite. The quantity of mismatch strains and C_B^{min} depends on the volume of the interstitial sites of the crystallite. Since the γ-phase has the larger interstitial sites than the α-phase, it can accommodate the nitrogen atoms with less distortion and lower volume mismatch. Therefore, the process of transformation of bcc to fcc can take place by progression of MA. Also, according to the previous investigations [7, 60], the fcc γ-phase has smaller interfacial energy, compared with the bcc α-phase, thereby enhancing the α-to-γ phase transformation. According to the result (Table 4), it can be seen that in the samples milled under the nitrogen atmosphere by increasing the milling time the amount of γ-phase increases and then decreases. It can be signified that during milling under nitrogen, in parallel with the ferrite-to-austenite phase transformation, the amorphization process developed progressively and both ferrite and austenite phases can be transformed into the amorphous phase. At the initial stages of the milling process, as the dissolved nitrogen is relatively low, the ferrite-to-austenite phase transformation is dominant and the percentage of austenite phase is increased by the milling time. By progression of MA and consequently increasing the dissolved nitrogen, the amorphization overcomes the ferrite-to-austenite phase transformation; hence, the amount of austenite is decreased.

Thermal stability

As mentioned in the "Results" section, in the samples milled under the nitrogen atmosphere, during the heating process (the DSC test), the γ-to-α phase transformation and the crystallization of the amorphous phase to a combination of α, CrN, and Cr_2N occur. There is no quaternary phase diagram in the literature to evaluate the phase stability in the Fe–Cr–Mn–N system. However, Qiu [61] proposed a thermodynamic model to evaluate the phase stability in this particular system. Our experimental results are compatible with this model, indicating the ferrite and nitride phases are the most stable phases at room temperature.

It should be mentioned that by progression of the MA process, due to an increase in the difficulty of crystallization of the amorphous phase, the crystallization temperature moves to the high-temperature side. The main contribution to these phenomena is the dissolved nitrogen atoms. The crystallization phenomenon needs the redistribution of the alloying elements to form critical nuclei. According to the following reasons, the infused nitrogen atoms can suppress the nucleation of crystalline phases from the amorphous phase and can, therefore, increase the crystallization temperature. The first reason is that the dissolved nitrogen increases the degree in dense random packing of the structure; hence, a decrease in the atomic diffusion coefficients occurs. The second reason is that the addition of the nitrogen atoms disrupts the short-range order of the structure and consequently suppresses the formation of crystal nuclei [62]. Thirdly, since the diameter of nitrogen atoms is much smaller than that of Fe, Cr, and Mn, this large difference in the atomic size suppresses the long-range interdiffusion required for the crystallization process [63]. Finally, due to the high affinity of the constituent elements (especially Cr) for N and the strong attractive bonding between the metal-nitrogen pairs, the nitrogen atoms are not apt to become each other's neighbors and subsequently are surrounded by the metallic atoms. The presence of these metal–nitrogen atomic pairs suppresses the atomic rearrangement required for the precipitation of the crystalline phases and a large chemical fluctuation to form the critical nuclei of the crystalline phases is required.

Conclusions

In this study, the MA process of the elemental Fe, Cr, and Mn powder mixtures under a nitrogen gas atmosphere resulted in the formation of high-nitrogen 74Fe18Cr8Mn alloys. It was found out that during the milling process, the nitrogen atoms diffuse down to the microstructure of the powders and by increasing the milling time, the nitrogen content rises to 2.54 wt% within 144 h. Under these conditions, the grain refinement occurs significantly and the material structure is transformed from a predominant α-phase into a mixture of γ and amorphous phases. The quantitative phase analysis and thermal stability studies showed that the amorphous phase appears within the first 24 h of milling, becoming the dominant phase by progression of MA. The amorphous phase content eventually reaches the value of 83.7 wt% within 144 h, being verified by the microscopic results. The comparison of the thermal and microstructural results with the quantitative phase analysis confirms the validity of the quantitative method used in this study. In addition, the thermal behavior studies demonstrated that the dissolved nitrogen atoms increase the thermal stability of the amorphous phase. This study has also revealed that during the milling process under an inert atmosphere like argon, the structure contains a predominant nanocrystalline α-phase and a trivial amount of amorphous phase. At this atmosphere, the grain refinement also occurs but not to such an extent as the samples milled under nitrogen. It signifies an essential contribution of nitrogen to the grain refinement and phase transformation

during MA of Fe–Cr–Mn alloys under the nitrogen gas atmosphere.

Acknowledgements The authors would like to thank Iran Alloyed Steel Company for LECO gas analysis. Shiraz University Research Council and Nanyang Technological University (NTU) are also acknowledged for their support to this study.

References

1. Nakada N, Hirakawa N, Tsuchiyama T et al (2007) Scr Mater 57:153
2. Sumita M, Hanawa T, Teoh SH (2004) Mater Sci Eng C 24:753
3. Balachandran G, Bhatia ML, Ballal NB et al (2001) ISIJ Int 41:1018
4. Fréchard S, Redjaïmia A, Lach E et al (2008) Mater Sci Eng A 480:89
5. Murakami R, Aoyama Y, Tsuchida N et al (2007) Mater Sci Forum 561–565:37
6. Cisneros MM, López HF, Mancha H et al (2002) Metall Mater Trans A 33:2139
7. Cisneros MM, López HF, Mancha H et al (2005) Metall Mater Trans A 36:1309
8. Méndez M, Mancha H, Cisneros MM et al (2002) Metall Mater Trans A 33:3273
9. Mancha H, Mendoza G, Belmares S et al (2001) Mater Sci Forum 360–362:189
10. Kataoka K, Tsuchiyama T, Goto H et al (2003) Trans Ind Inst Metal 56:527
11. Enayati MH, Bafandeh MR (2008) J Alloys Compd 454:228
12. Jiang JZ, Gente C, Bormann R (1998) Mater Sci Eng A 242:268
13. Zhu LH, Huang QW, Zhao HF (2004) Scr Mater 51:527
14. Suryanarayana C (2001) Prog Mater Sci 46:1
15. Wagner CNJ, Boldrick MS (1993) J Alloys Compd 194:295
16. Johnson WL (1988) Mater Sci Eng 97:1
17. Chattopadhyay PP, Samanta A, Lojkowski W et al (2007) Metall Mater Trans A 38:2298
18. Shen G, Jiang DM, Lin F et al (2005) Physica B 367:137
19. Du SW, Ramanujan RV (2005) J Magn Magn Mater 292:286
20. Popa F, Isnard O, Chicinas I et al (2007) J Magn Magn Mater 316:e900
21. Shaham D, Rawers J, Zolotoyabko E (1996) Mater Lett 27:41
22. Munitz A, Kimmel G, Rawers JC et al (1997) Nanostruct Mater 8:867
23. Rawers JC, Govier D, Doan R (1996) Mater Sci Eng A 220:162
24. Koyano T, Takizawa T, Fukunaga T et al (1993) Jpn J Appl Phys 32:1524
25. Ogino Y, Murayama S, Yamasaki T (1991) J Less-Common Met 168:221
26. Ogino Y, Yamasaki T, Murayama S et al (1990) J Non-Cryst Solids 117–118:737
27. Miura H, Omuro K, Ogawa H (1996) ISIJ Int 36:951
28. Aoki K, Memezawa A, Masumoto T (1992) Appl Phys Lett 01(9):1037
29. Fukunaga T, Ishikawa E, Koyano T et al (1995) Physica B 213–214:526
30. Fukunaga T, Kuroda N, Lee CH et al (1994) J Non-Cryst Solids 176:98
31. Winburn RS, Grier DG, Mccarthy GJ et al (2000) Powder Diffr 15:163
32. De La Torre AG, Bruque S, Aranda MAG (2001) J Appl Cryst 34:196
33. Kemethmüller S, Roosen A, Goetz-Neunhoeffer F et al (2006) J Am Ceram Soc 89:2632
34. Gualtieri ML, Prudenziati M, Gualtieri AF (2006) Surf Coat Technol 201:2984
35. Whitfield PS, Mitchell LD (2003) J Mater Sci 38:4415. doi: 10.1023/A:1026363906432
36. Fecht HJ (1995) Nanostruct Mater 6:33
37. Yelsukov EP, Dorofeev GA, Zagainov AV et al (2004) Mater Sci Eng A 369:16
38. Mohamed FA (2003) Acta Mater 51:4107
39. Eckert J, Holzer JC, Kill CEIII et al (1992) J Mater Res 7:1751
40. Zhao YH, Zhu YT, Liao XZ et al (2007) Mater Sci Eng A 463:22
41. Buffington FS, Cohen M (1954) Acta Metall 2:660
42. Borg RJ, Diens G (1988) Solid state diffusion. Academic Press, Boston, p 80
43. Lin S, Ledbetter H (1993) Mater Sci Eng A 167:81
44. Ledbetter HM, Austin MW (1985) Mater Sci Eng 70:143
45. Mohamed FA, Xun Y (2003) Mater Eng A 358:178
46. Schramm RE, Reed RP (1975) Metall Trans A 6:1345
47. Stoltz RE, Van der Sande JB (1980) Metall Trans A 11:1033
48. Dulieu D, Nutting J (1964) Iron Steel Inst 86:140
49. Kibey S, Liu JB, Curtis MJ, Johnson DD et al (2006) Acta Mater 54:2991
50. Jiang B, Qi X, Zhou W et al (1996) Scr Mater 34:1437
51. Fujikura M, Takada K, Ishida K (1975) ISIJ Int 15:464
52. Yakubtsovi A, Ariapour A, Perovic DD (1999) Acta Mater 47:1271
53. Gavriljuk V, Petrov Y, Shanina B (2006) Scr Mater 55:537
54. Byranes MLG, Grujicic M, Owen WS (1987) Acta Metall 35:1853
55. Werner E (1998) Mater Sci Eng A 101:93
56. Nieh TG, Wadsworth J (1991) Scr Metall 25:955
57. Egami T, Waseda Y (1984) J Non-Cryst Solid 64:113
58. Van der Kolk GJ, Miedema AR, Niessen AK (1988) J Less-Common Met 145:1
59. Nishizawa T (1973) Bull Jpn Inst Met 12:401
60. Meng Q, Zhou N, Rong Y et al (2002) Acta Mater 50:4563
61. Qiu C (1993) Metall Trans A 24:2393
62. Weber TA, Stillinger FH (1985) Phys Rev B 31:1954
63. Sharma S, Suryanarayana C (2008) J Appl Phys 103:013504-1